processes

MDPI

Article

Capacity Management in Smart Grids Using Greedy Randomized Adaptive Search Procedure and Tabu Search

Hugo de Oliveira Motta Serrano, Cleberton Reiz * and Jonatas Boas Leite

Department of Electrical Engineering, Faculty of Electrical Engineering, Sao Paulo State University, Campus of Ilha Solteira, São Paulo 15385-000, Brazil; hugo.motta@unesp.br (H.d.O.M.S.); jb.leite@unesp.br (J.B.L.)
* Correspondence: cleberton.reiz@unesp.br

Abstract: Over time, distribution systems have progressed from small-scale systems to complex networks, requiring modernization to adapt to these increasing levels of active loads and devices. It is essential to manage the capacity of distribution networks to support all these new technologies. This work, therefore, presents a method for evaluating the impact of optimal allocation and sizing of DGs and load shedding for response demand programs on distribution networks to improve the reliability and financial performance of electric power systems. The proposed optimization tool uses the Greedy Randomized Adaptive Search Procedure and Tabu Search algorithms. The combined optimization of DG allocation simultaneously with load shedding, reliability indices, load transference, and the possibility of islanded operation significantly improves the quality of the planning proposals obtained by the developed method. The results demonstrate the efficiency and robustness of the proposed method, improving the voltage profile by up to 2.02%, relieving the network capacity, and increasing the load restoration capability and reliability. Statistical analysis is also carried out to highlight the performance of the proposed methodology.

Keywords: distribution network; capacity management; GRASP; Tabu Search; distributed generator; load shedding

Citation: Serrano, H.d.O.M.; Reiz, C.; Leite, J.B. Capacity Management in Smart Grids Using Greedy Randomized Adaptive Search Procedure and Tabu Search. *Processes* **2023**, *11*, 2464. https://doi.org/10.3390/pr11082464

Academic Editors: Dimitris Ipsakis and Andreas Yiotis

Received: 6 July 2023
Revised: 8 August 2023
Accepted: 9 August 2023
Published: 16 August 2023

1. Introduction

The distribution networks must supply the load demand that varies daily and seasonally. Since the demand is largely unpredictable, and making programmable interruptions is not a good option because of its very high cost, the generation system capacity must be capable of supplying the maximum demand or peak demand [1]. The management of these resources becomes increasingly important due to distributed energy resources (DERs) integration into the grid. The active and reactive power injected by DERs into the grid not only affects the local voltage but can also influence charging conditions and power flow on the network [1]. Distribution networks can experience a significant increase in peak loads, which, in the absence of smart functionality to reduce them, may result in a substantial investment increase in network infrastructure [2]. An adequate management mechanism is thus necessary to optimize the use of the network's capacity, ensuring sustainable and more efficient distribution systems [2].

The installation of a distributed energy resource management system (DERMS) can aid network operations performed using the advanced distribution management system (ADMS) [3]. This strategy can significantly reduce the uncertainties caused by dispersed DERs that may not follow a unified or coordinated pattern of operation. The integration of DERMS and ADMS provides, additionally, the operability of programs for demand-side management (DSM).

The concept of demand-side management emerged in the 1980s as a response to the unpredictable growth in demand for electricity in that period. The development of a broad market based on real-time demand and supply data was a result of this situation. Future

consumer demand used to be handled traditionally. However, with the introduction of this concept, fluctuations and variations in energy demand began to be better accommodated to deal with future uncertainties [4].

The implementation of demand-side management increases the complexity of power systems since the adequate performance of demand-side management requires monitoring the loads and generators of the system [5]. With this, additional expenses are generated with the incentive to participate in demand-side management programs. The benefits of demand-side management far outweigh its disadvantages [6]. The DSM has become essential in implementing smart grids, especially in the residential sector, as it significantly contributes to reducing the peak of electricity demand.

Some studies have been carried out on this subject in recent years, such as [7], which applies the Optimal Power Flow (OPF) technique in distribution networks to maximize system benefits by considering the capacity of loads, by assessing the optimal allocation of demand-side resources, and by providing ancillary services like an operational reserve. The authors of [8] developed a procedure to determine the best buses for demand response based on distribution factors, power transfer, available transfer capacity, and optimal power flow. The results help reduce line congestion, increase benefits for customers and the independent system operator, and avoid line interruptions and blackouts, thus increasing system reliability.

The DSM has been strategically used by aggregators and power utilities to manage energy consumption through incentives. Such incentives include reducing electricity tariffs when aggregated demand is below average. The goal is to encourage the final consumer to move flexible loads for such periods [9].

Demand-side management takes three different approaches: strategic load growth, energy efficiency, and demand response [4,6]. In this work, the demand response is applied, which, according to [10], refers to changes in the electricity consumption patterns of end-users in response to changes in electricity prices over time or incentives offered to reduce electricity use during periods of high wholesale market prices or compromised system reliability.

Several recent kinds of research have been carried out regarding the demand response [11–13] to minimize the load curve, considering the presence of DGs. The authors of [11] considered both demand-side management and network reconfiguration simultaneously. The mathematical model's objective function seeks to minimize the total cost over the planning horizon, encompassing DG's investment, operation, fuel, and demand-side management costs. The model is converted into a three-tier programming model, and optimal DG planning results are achieved by using a hybrid solution strategy.

To deal with the problem of photovoltaic and wind energy consumption and minimize the total cost of energy purchase, an optimal real-time dispatch model is established in [12], considering the grid security constraints and supply and demand constraints to ensure safe network operation. The authors of [13] addressed a priority-based load shifting to bridge the gap between demand and supply. The power consumer can then cooperate with the utility by managing its demand, that is, by scheduling flexible appliances based on consumption priority.

Network reconfiguration can include the possibility of islanded operation to increase network reliability. During a fault event, the closest protection device to the fault trips, isolating the downstream sections to minimize the number of customers de-energized [14]. DG integration allows the restoration of downstream feeder sections, with part of distribution network loads, by forming microgrids. Such a strategy reduces the number of customers de-energized and increases restoration capacity and reliability indexes and the profit of distribution companies. The authors of [14] performed demand-side management through the hosting capacity of a meshed distribution network using the Repeating Particle Swarm metaheuristic under a 123-bus network with the integration of multiple and large-scale photovoltaic systems.

Recent works in the literature have focused on the demand response strategy to reduce the load flows through the distribution lines by avoiding network congestion and, thus, improving the system's reliability [15–18]. In [15], the frequency-based load shedding using the polynomial regression method and mixed integer linear programming (MILP) is applied as a demand response. The MILP is used for the ideal location of non-vital loads, discarding them to ensure the functionality of critical loads.

The authors of [16] reviewed load-shedding schemes in distribution networks considering DGs. This paper reports that the conventional technique is a trial-and-error procedure used to develop the number and size of load reduction steps. An adaptive technique is proposed to improve the power imbalance estimation and determine the optimal location of the load to be eliminated. The computational intelligence techniques are based on Artificial Neural Networks, metaheuristics, and Fuzzy Logic using the under-frequency load shedding scheme (UFLS) and the voltage shedding scheme. In [17], the UFLS technique based on the combination of Particle Swarm Optimization (PSO) and Bacterial Foraging (BF) metaheuristics was proposed to reduce the amount of disconnected load and increase the lowest possible oscillation frequency.

The authors of [18] identify DG's optimal size and location with a minimum cost as demand response through the simulated annealing (SA) metaheuristic to a microgrid to achieve the stipulated reliability criteria. In [19], a mixed integer nonlinear programming (MINLP) is proposed, minimizing the system's annual energy losses, while [20] proposes a mixed-integer quadratically constrained programming problem, solving using a genetic algorithm (GA).

However, none of these works considered the optimal allocation of DGs simultaneously with load shedding for power loss minimization and, consequently, the total cost of the distribution network, improving reliability through capacity management. In contrast to works that manage the demand side through the hosting capacity or just cut the load on the network without considering the optimal allocation of a distributed generator, this work presents the following contributions:

- The study and problem definitions of the operation and management of DGs, simultaneously with load shedding, to manage the capacity of distribution networks;
- Use of metaheuristics Greedy Randomized Adaptive Search Procedure (GRASP) with Tabu Search (TS) to solve the proposed problem of distribution network capacity management;
- Statistical analysis to validate the proposed formulation and solution technique, promoting the proper integration of DERs into the electrical grids and, thus, maximizing their benefits and maintaining the quality of supply and the reliability of the electrical distribution system.

This paper is set out as follows. Section 2 describes the mathematical modeling of the problem. Section 3 presents the solution techniques using GRASP and TS metaheuristics. Section 4 presents the numerical results, and Section 5 presents the conclusions.

2. Materials and Methods

Power losses are intrinsic conditions of power energy systems and directly impact their performance. Nevertheless, there are several techniques to reduce them, increasing the voltage profile and energy quality. Optimal DG allocation and sizing have the potential to improve the power system performance, providing decentralization of energy sources, power loss reduction, and postponement in reinforcement investments. The integration of DGs in the distribution system also enables the islanded operation. Thus, during a fault event, the network reconfiguration allows DGs to remain in operation as a microgrid, improving the energy quality by reducing the power outage. Figure 1a highlights such a strategy, where DG1 and DG2 can supply loads nearby.

The DSM also improves power system performance by using load shedding. This scheme gives customers the option of a low-cost service, where the load shedding is a condition of their contract type. The DSM relieves capacity and increases load restoration.

In this way, during a fault event, the load shedding can also be advantageous by increasing the chance of islanded operation and load transference to neighboring feeders, as shown in Figure 1b.

The management of the network capacity, sizing and locating of DGs, and load shedding were carried out using the solution of an optimization model. Figure 2 shows an abstract of the proposed methodology, highlighting some advantages of optimal DG planning and demand-side management.

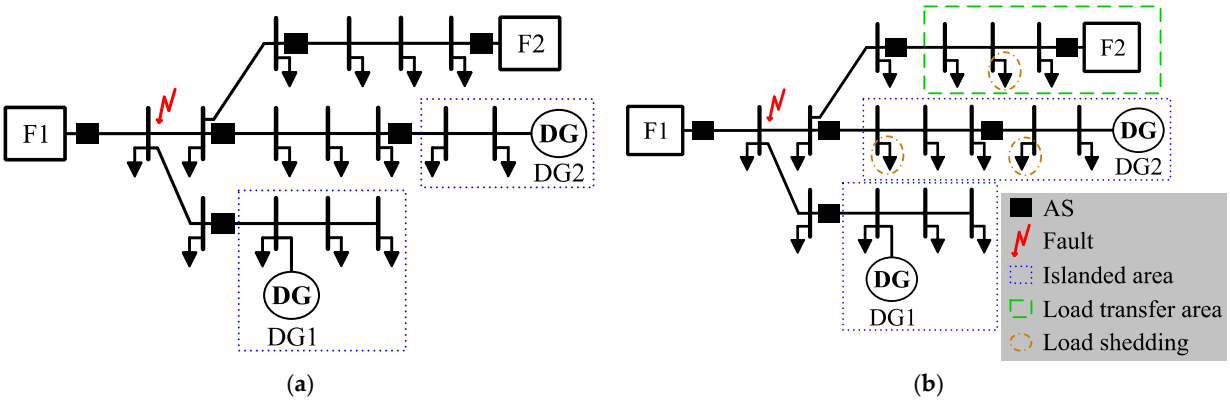

Figure 1. Benefits of applying several strategies for improving energy quality and hosting capacity: (**a**) using only the islaned operation and (**b**) combining islanded operation with load shedding and load transference to neighbor feeders.

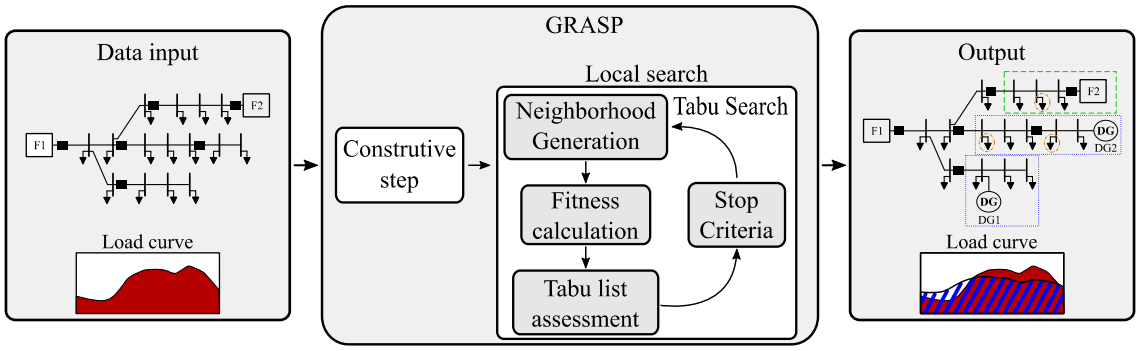

Figure 2. Graphical abstract highlighting the whole process using the proposed method.

2.1. Objective Function

Comprising three elements, the objective function in (1) is composed as follows: cost of losses C^{LOSS}, cost of load shedding C^{SHED}, and cost of energy not supplied C^{ENS}.

$$OF = C^{LOSS} + C^{SHED} + C^{ENS} \tag{1}$$

The distribution network losses are determined as given by (2), assuming the cost of losses for a horizon of one year [21], where k_e is the cost of losses, $I_{j,p,y}$ is the current flow, and $R_{j,p}$ is the resistance of the j-th distribution line at the p-th phase to a distribution network with nl lines. Each year of the planning horizon is represented by y from the set $\boldsymbol{\varphi}$. The cost of load shedding is represented by (3), where $X_{i,p,k,y}$ is the percentage of load shedding; $P^{MAX}_{i,p,k,y}$ is the maximum cuttable power in i-th bus and p-th phase to a distribution network with nb buses; and C^{SHED}_{k} is the cost of load shedding to the k-th type of customer, which can be residential, R, commercial, C, or industrial, I.

$$C^{LOSS} = k_e \sum_{y \in \boldsymbol{\varphi}} \sum_{j=1}^{nl} \sum_{p \in \{a,b,c\}} \left| I_{j,p,y} \right|^2 R_{j,p} \tag{2}$$

$$C^{SHED} = \sum_{y \in \boldsymbol{\varphi}} \sum_{i=1}^{nb} \sum_{p \in \{a,b,c\}} \sum_{k \in \{R,C,I\}} \left(X_{i,p,k,y} P_{i,p,k,y}^{MAX} C_k^{SHED} \right) \tag{3}$$

The cost of energy not supplied considering the indices of permanent faults is given by (4). We assume that a section is defined as a set of branches and buses belonging to a device's protective zone. More details can be found in [22].

$$C^{ENS} = \sum_{k \in \{R,C,I\}} C_k^{ENERGY} \sum_{y \in \boldsymbol{\varphi}} \frac{P_y^{ENS}}{(1 + IRR)^y} \tag{4}$$

In (4), C_k^{ENERGY} is the energy price according to the type of customer, P_y^{ENS} is the energy not supplied during permanent faults for each year y of the planning horizon $\boldsymbol{\varphi}$, and IRR is the internal rate of return. In (5), the estimation of interrupted energy P_y^{ENS} depends on the failure rate λ_h^p for permanent faults and the length of each branch h belonging to the set of branches from section i, $\boldsymbol{\pi}_i$. The total loads in section i and downstream are represented by $P_{i,y}^p$, during year y. The set $\boldsymbol{\beta}$ includes all sections defined by the protection and control devices.

$$P_y^{ENS} = \sum_{i \in \boldsymbol{\beta}} \sum_{h \in \boldsymbol{\pi}_i} \left(\lambda_h^p L_h \right) \left[\left(P_{i,y}^p - P_{i,y}^{MG} - P_{i,y}^{TS} \right) t_R^p + P_{i,y}^{TS} t_{SW} \right] \tag{5}$$

$$P_{i,y}^{MG} = \sum_{m \in \boldsymbol{M}} P_{i,y,m}^{MG} \tag{6}$$

$$P_{i,y,m}^{MG} = 0, \;\; f = h \; \forall \; h \in \boldsymbol{\sigma}_m \tag{7}$$

$$P_{i,y}^{TS} = \sum_{w \in \boldsymbol{W}} P_{i,y,w}^{TS} \tag{8}$$

$$P_{i,y,w}^{TS} = 0, \;\; f = h \; \forall \; h \in \boldsymbol{\tau}_w \tag{9}$$

During a fault event, the islanded operation can occur, depending on the power balance available between loads and DGs in each section. $P_{i,y}^{MG}$ is the microgrids' loading that can be restored, as given in (6). This expression is the sum of loads $P_{i,y,m}^{MG}$ within the microgrid m from the set $\boldsymbol{M}$. For a fault inside the microgrid, that is, a fault in a branch $h \in \boldsymbol{\sigma}_m$, or when the microgrids' loading is bigger than DG capacity, the islanded operation cannot be performed, and DGs must be disconnected, as given in (7).

The same occurs for load transference to neighbor feeders. $P_{i,y}^{TS}$ represents the sum of transferred loads downstream automatic tie switches in section i. Such estimation is based on the sum of all loads that can be restored by using each automatic tie switch from the set $\boldsymbol{W}$ (8). For a fault within $\boldsymbol{\tau}_w$ or when the sum of transferred loads is bigger than the neighbor feeder capacity, the load transference cannot be performed, as given in (9). The duration of power outages caused by permanent faults is denoted as t_R^p, while t_{SW} is the time of power outage necessary for the system operator to restore the loads using automatic switches.

2.2. Constraints Set

The active and reactive power balance equations for each bus of radial networks are, respectively, represented by equality constraints (10) and (11). The voltage magnitude limits of the i-th bus are represented by constraint (12), while the current flow limits for each phase, $I_{p,i,y}$, are represented by (13), with an upper limit of $\overline{I_p}$. Active and reactive

power of DGs must not exceed upper and lower boundaries as, respectively, given by constraints (14) and (15).

$$P_{p,i,y}(V,\theta) - P^{DG}_{p,i,y} + P^{D}_{p,i,y} = 0, \ \ \forall i \in nb, \ y \in \boldsymbol{\varphi}, \ p = a,b,c \tag{10}$$

$$Q_{p,i,y}(V,\theta) - Q^{DG}_{p,i,y} + Q^{D}_{p,i,y} = 0, \qquad \forall i \in nb, \ y \in \boldsymbol{\varphi}, \ p = a,b,c \tag{11}$$

$$\underline{V_p} \leq V_{p,i,y} \leq \overline{V_p}, \ \ \forall i \in nb, \ y \in \boldsymbol{\varphi}, \ p = a,b,c \tag{12}$$

$$0 \leq I_{p,i,y} \leq \overline{I_p}, \ \ \forall i \in nb, \ y \in \boldsymbol{\varphi}, \ p = a,b,c \tag{13}$$

$$\underline{P^{DG}} \leq P^{DG}_{p,i,y} \leq \overline{P^{DG}}, \ \ \forall i \in nb, \ y \in \boldsymbol{\varphi}, \ p = a,b,c \tag{14}$$

$$\underline{Q^{DG}} \leq Q^{DG}_{p,i,y} \leq \overline{Q^{DG}}, \ \ \forall i \in nb, \ y \in \boldsymbol{\varphi}, \ p = a,b,c \tag{15}$$

3. Solution Technique

The proposed optimization model, a mixed integer nonlinear programming model, is solved using the GRASP metaheuristic with TS in the local search phase. It combines the advantages of two widely known techniques, speeding up the search process with the greedy stage of GRASP and reducing the chances of becoming stuck in local minima due to the flexibility provided by the tabu list of prohibited solutions.

The GRASP metaheuristic consists of two phases: constructive and local search, performed sequentially and iteratively [23]. In the first phase, different initial greedy and random solutions are generated. This step directs the method to regions more likely to obtain local optima, accelerating the exploration process. Then, the found solutions are refined in the local search phase using the TS algorithm [24], improving them even more.

The tabu list restricts the choice of solutions that have been visited recently. Then, the optimization process allows the TS to select worse-quality solutions for local exploration. Such an aspect allows for extensive exploration, obtaining local optimal solutions from different regions of the search space. From left to right, Figure 3 shows the basic flowchart of GRASP and TS.

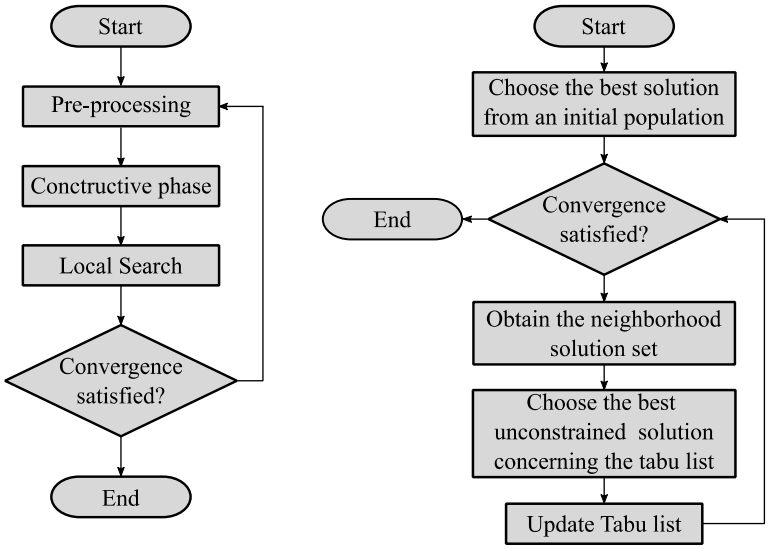

Figure 3. Basic flowcharts of GRASP and TS.

In this work, the convergence criterion is based on the iteration number. The algorithm repeats up to a limit of iterations, or if the sequence of iterations without improvement reaches a certain limit, both previously defined by the user.

3.1. Codification

In coding the individuals for the generators, a set of real numbers is used, in which the integer part characterizes the active power $P_{j,y}^{DG}$ of the DG, and the decimal part represents the power factor $pf_{j,y}$ of the generator, which must be equal to or higher than $\underline{pf}$. If an i-th bus has allocated the j-th DG, $P_{i,y}^{DG} = P_{j,y}^{DG}$ and $Q_{i,y}^{DG} = P_{j,y}^{DG}\left(1 - pf_{j,y}^{2}\right)^{1/2} / pf_{j,y}$. In (16) and (17), $\alpha_{j,y}$ and $\beta_{j,y}$ are integer random numbers that vary from 0 to $\overline{\alpha}$ and $\overline{\beta}$, respectively. Increments in active power and power factor are ΔP^{DG} and Δpf. As for the load shedding, in (18), integer values represented by the variable $\gamma_{j,y}$ from 0 to $\overline{\gamma}$ are used to characterize the percentage of load shedding $X_{j,y}$.

$$P_{j,y}^{DG} = \alpha_j \Delta P^{DG}, \;\; \alpha_{j,y} = 0, 1, \ldots, \overline{\alpha} \tag{16}$$

$$pf_{j,y} = \underline{pf} + \beta_{j,y} \Delta pf, \;\; \beta_{j,y} = 0, 1, \ldots, \overline{\beta} \tag{17}$$

$$X_{j,y} = \gamma_j \Delta X, \;\; \gamma_{j,y} = 0, 1, \ldots, \overline{\gamma} \tag{18}$$

Figure 4 presents the coding of a candidate solution as a vector where each element is associated with the position of the buses DG_n and LS_n for generator allocation and load shedding, respectively, where n represents the number limit of each one. Figures 5 and 6 display detailed flowcharts of the whole proposed method.

DG_0	...	DG_n	LS_0	...	LS_n
$P_{0,0}^{DG} . pf_{0,0}$	...	$P_{n,y}^{DG} . pf_{n,y}$	$X_{0,0}$	...	$X_{n,y}$
n DGs $\forall\, y \in \boldsymbol{\varphi}$			n LOAD SHEDDING $\forall\, y \in \boldsymbol{\varphi}$		

Figure 4. Coding vector of a candidate solution.

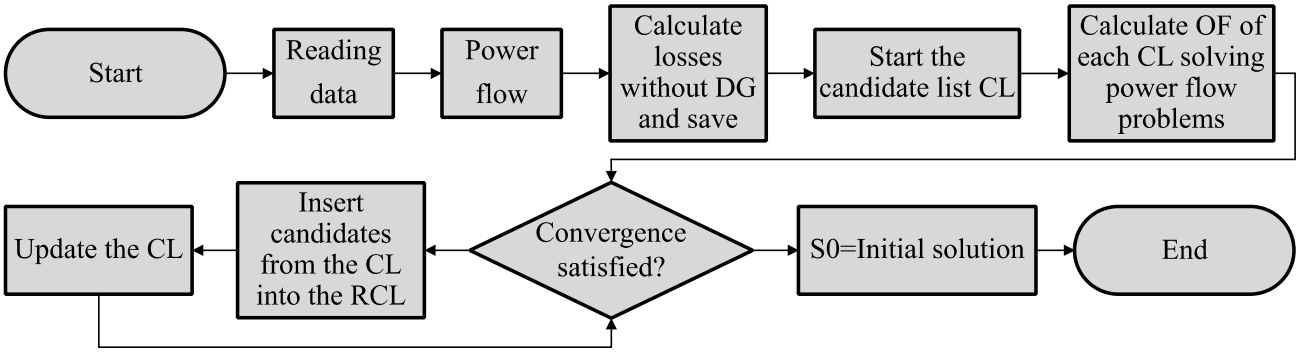

Figure 5. Constructive step flowchart.

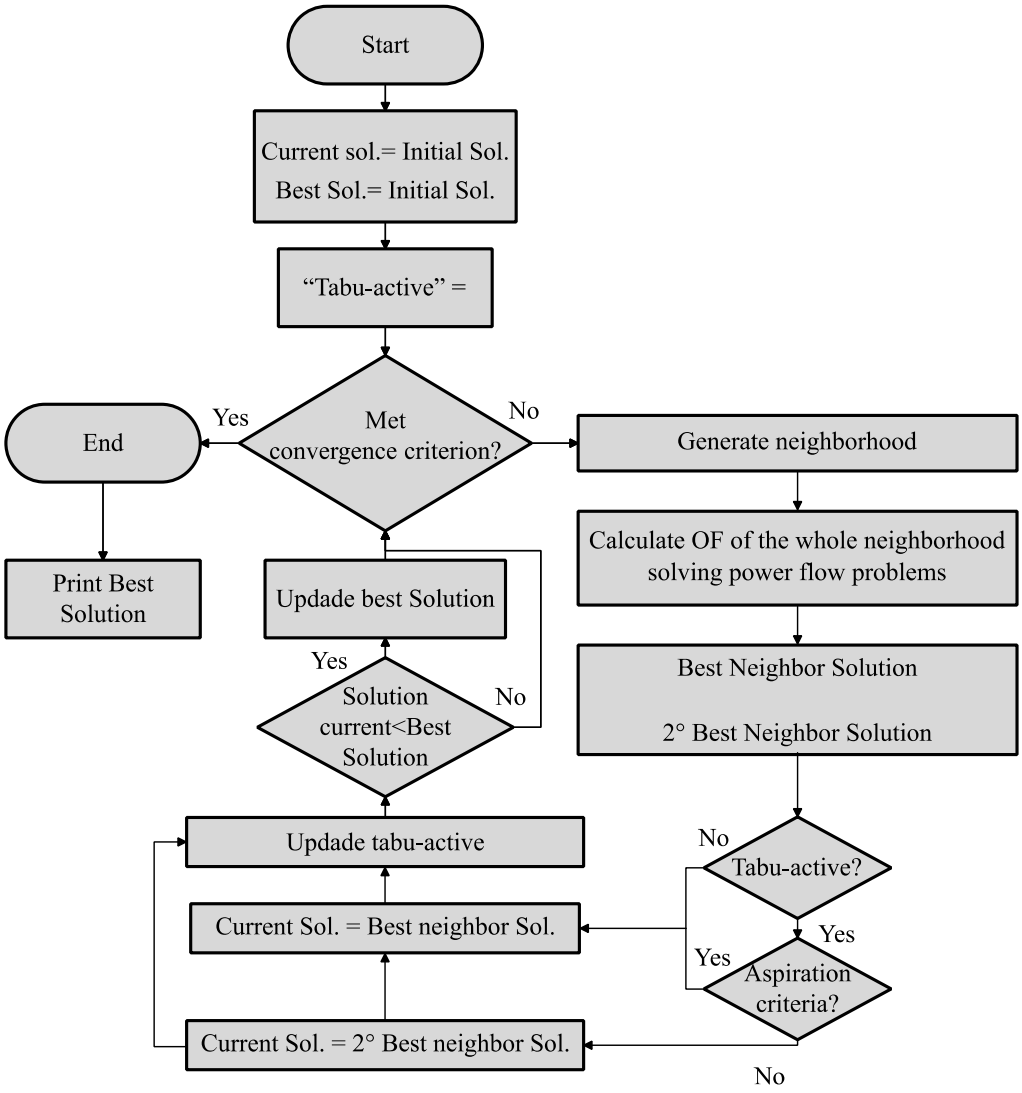

Figure 6. Local search phase flowchart.

3.2. Constructive

During the constructive phase, as depicted in Figure 5, the pre-processing stage is initiated, which involves running a three-phase power flow analysis. This analysis provides the voltage profile for every phase at all buses, current flows through branches, and the sum of losses concerning the feeder under study. The power flow analysis ensures the active and reactive power balance, as specified by constraints (10) and (11). A set of candidate buses with the lowest voltages and highest demand is chosen after power flow estimation for DG allocation and load shedding.

The initial candidate construction occurs by inserting elements one by one from the solution of the search space (CL). The search space is narrowed down afterward based on Equation (19), resulting in a list called the restricted candidate list (RCL), which includes the top-performing candidates. An element is randomly selected in each iteration to be included in the candidate solution under the building process.

$$\underline{g(c)} \leq g(c) \leq \underline{g(c)} + a\left[\overline{g(c)} - \underline{g(c)}\right] \tag{19}$$

GRASP has a greedy function $g(c)$ to assess candidate solutions c, providing the cost concerning the addition of an element to the initial solution. Assuming a problem of minimization, the solutions with the lowest and greatest cost among candidates in the CL

are, respectively, represented as $\underline{g(c)}$ and $\overline{g(c)}$. A candidate c in the CL is placed in the RCL if and only if (19).

3.3. Local Search Phase

The TS metaheuristic is employed in this stage to enhance the solution obtained from the constructive process. As depicted in Figure 6, the search traverses the neighborhood of the current configuration, locating the setup that enhances the objective function's value. The algorithm's performance is dependent on the quality of these configurations.

After computing the objective function's values throughout the neighborhood, the configuration with the lowest objective function value is chosen. Solutions from the Tabu list are compared with the chosen one. If it is, the algorithm assesses the aspiration criterion, verifying if the solution meets such criteria. The main objective is to remove the prohibition on the attribute of a high-quality neighboring solution that shares the same configuration as a previously visited solution. If the objective function value of the discovered neighboring solution is superior to that of the current solution, the restriction is revoked, and the transition is executed. In contrast, if the aspiration criterion is not satisfied, the configuration with the second-lowest objective function value is chosen.

4. Numerical Results and Discussion

The tests were performed on a real-world distribution feeder with 1806 buses [25], providing power to 834 loads, 781 in the low-voltage network, 53 in the medium-voltage network, and 47 distribution transformers. This test system has 11 automatic switches used for service restoration.

Smart grid customers are classified into residential (R), commercial (C), and industrial (I), where each type represents 50%, 30%, and 20% of distribution network loads. The cost of losses is defined as $k_e = 0.04$ USD/kWh [19]. Other optimization settings and parameters are shown in Table 1. The maximum capacity for each DG installed is 3.6 MW. The objective function proposed in (1) is penalized whenever constraints are violated during the solutions assessment. In the constructive phase, there are limiting parameters ΔP^{DG}, $\overline{\alpha}$, $\underline{pf}$, Δpf, and $\overline{\beta}$, ΔX and $\overline{\gamma}$, also shown in Table 1. ENS and load-shedding costs are based on [22] and [11], respectively. This work considers a planning horizon of one year.

Table 1. Optimization settings and parameters.

Parameters	Value	Parameters	Value	Parameters	Value
C_R^{SHED}	0.04 USD/kWh	C_R^{ENS}	1.5 USD/kWh	$\overline{\alpha}$	5
C_C^{SHED}	0.03 USD/kWh	C_C^{ENS}	3.0 USD/kWh	$\overline{\beta}$	9
C_I^{SHED}	0.02 USD/kWh	C_I^{ENS}	4.64 USD/kWh	$\overline{\gamma}$	5
$\underline{V}$	0.95 pu	$\overline{V}$	1.05 pu	$\underline{pf}$	0.90
ΔX	4%	ΔP^{DG}	160 kW	Δpf	0.01

To our best knowledge, there is no similar work in the literature that includes all aspects addressed in this paper. The proposed methodology's performance is evaluated using statistical analysis. Table 2 shows results from the statistical analysis, while Tables 3 and 4 highlight DG configuration and load shedding found by the worst solution, in that order.

Table 2. Statistical analysis.

a	*CVP*	$\overline{OF}$ (MUSD)	*TA* (MUSD)	*SD* (MUSD)
0.0	10.2	5.545	1.832	0.566
0.2	14	5.619	2.510	0.788
0.8	6	5.268	1.461	0.321
1.0	17	5.715	2.692	0.973

Table 3. Worst solution: DG configuration.

DG_n (bus)	13388	13446	13418	13392	13428	14120
α_n	4	0	0	0	0	0
P_n^G (kW)	640	0	0	0	0	0

Table 4. Worst solution: load shedding setup.

LS_n (bus)	200800	201128	201131	200914	201134	202004
γ_n	4	0	0	0	0	0
X_n	16%	0	0	0	0	0

In the simulations performed in the constructive phase, the twelve candidate buses are selected based on their position in a sequential manner. First, adjustments were made to find the solution with the most adequate value for the initial solution. Thus, we obtained Pearson's coefficient of variation (CVP), the average of objective functions (OF_{μ}), standard deviation (SD), and total amplitude (TA).

When analyzing Table 2, we can see that the most homogeneous solution was the one in which the algorithm is near random ($a = 0.8$), that is, with a variation of 6% in its solutions. The worst solution was obtained when the constructive phase was purely greedy ($a = 0.0$). In addition, if the solution is completely random ($a = 1.0$), the initial solution may not be very good, causing the algorithm to stop at a local optimum in the neighborhood search, which can generate more heterogeneous solutions. The algorithm stops when one of two conditions is met: either the incumbent solution does not improve for 300 generations, or it reaches the maximum number of 800 generations. In either case, the incumbent solution is considered the best-found solution.

Fifty simulations were performed to evaluate the performance of the algorithm with the results obtained during the tests, i.e., $a = 0.8$. Figures 7–9 are related to the statistical analysis of results provided by the proposed method, where each one shows a probability graph of objective functions, a box diagram with the scattering of objective functions, and the objective function histogram, in that order.

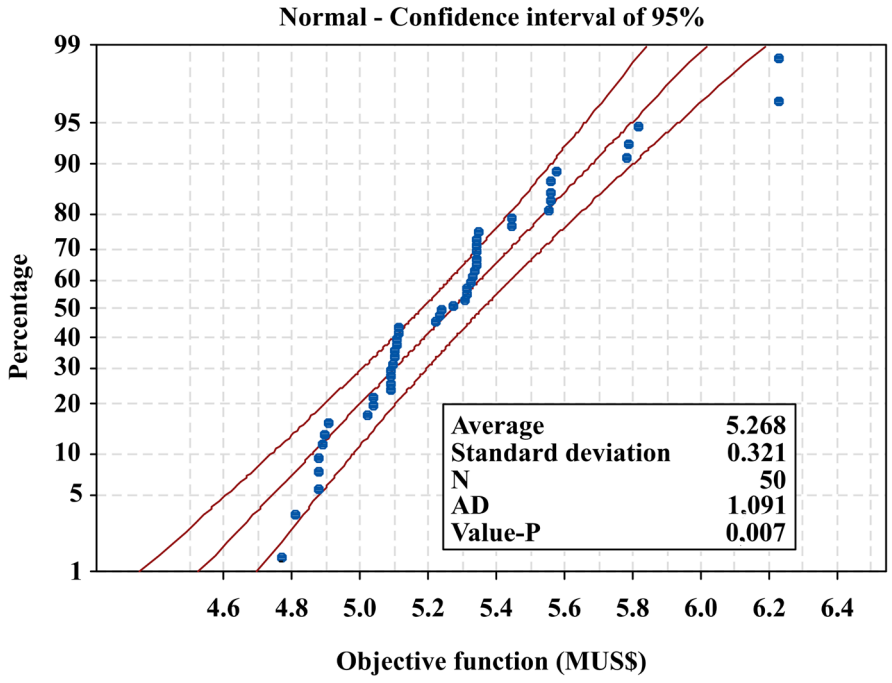

Figure 7. Probability graph of objective functions.

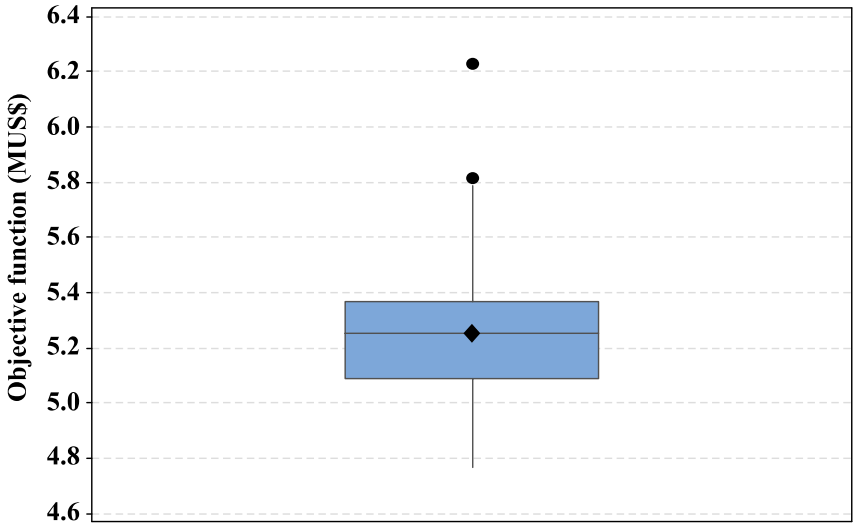

Figure 8. Box diagram: scattering of objective functions.

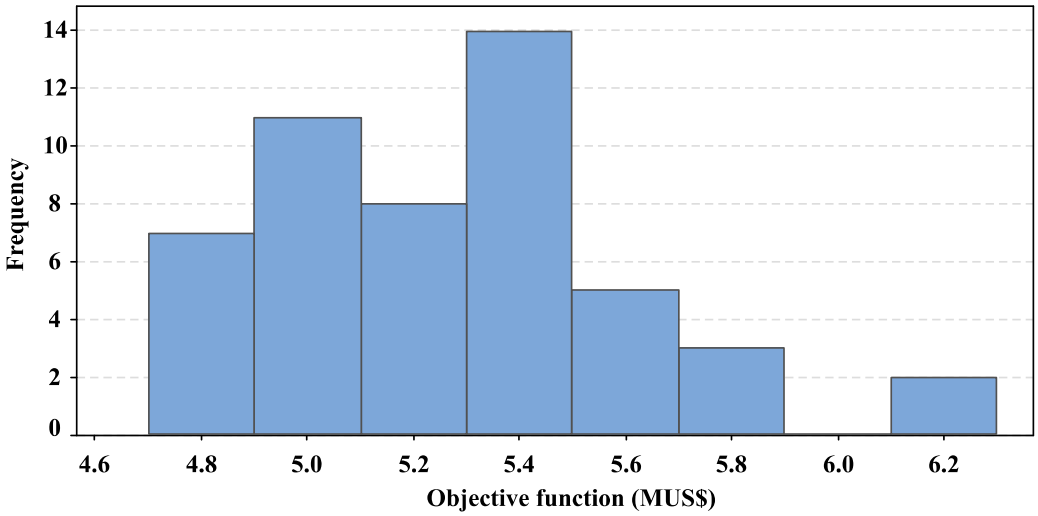

Figure 9. Objective function histogram.

The graph in Figure 8 shows that most of the data are on the right side. The symbol in the center represents the average value of MUSD 5.268, and the line represents the middle value of MUSD 5.251. Finally, 75% of all values are below the third quartile of MUSD 5.369. The graph shows two outliers (atypical value), which is because these solutions do not have any load shedding and have only installed a 640 kV generator, as shown in Tables 3 and 4.

The data do not follow a normal distribution because two solutions presented the value of the objective function as very high, with a much greater amplitude than the others, and the *p*-value is less than the significance level of 0.05, as shown in Figure 7.

From the histogram of the objective functions in Figure 9, we can see that the data are multimodal and have outliers since two solutions have only one DG installed, and the load cut has not been performed.

A diagram of the test system is shown in Figure 10, including DGs and the load-shedding locations. Low-voltage loads have been omitted from the figure. The dashed grey area shows an example of the low-voltage loads downstream of a distribution transformer. The positions of the worst DG and load-shedding setup are highlighted in red, while the best DG and load-shedding setup are emphasized in green.

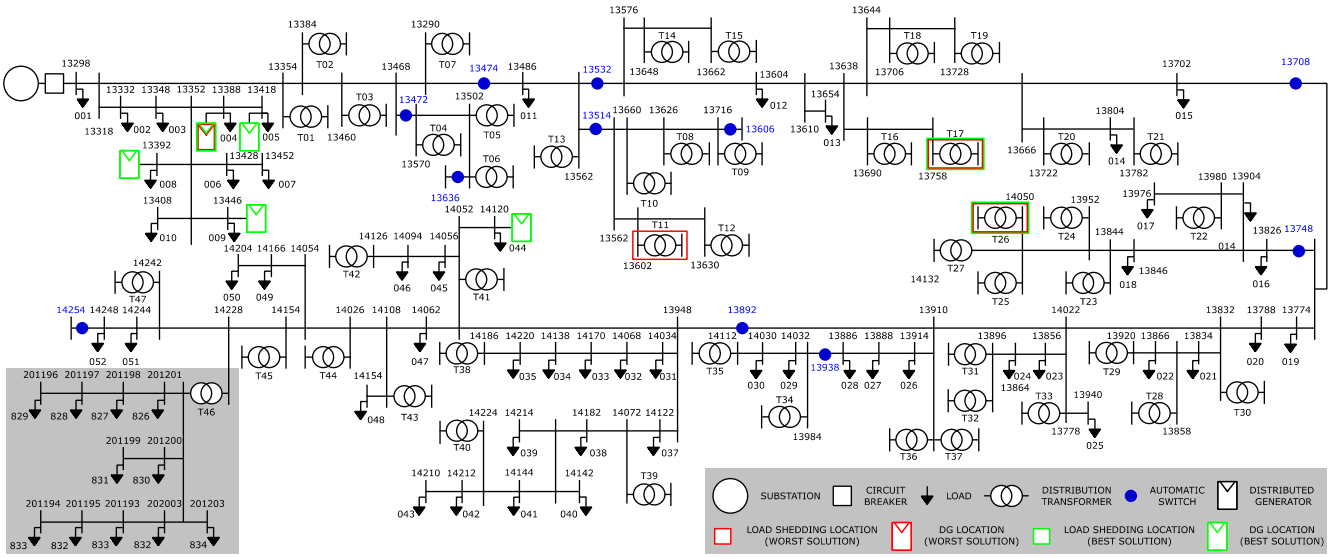

Figure 10. Test system, including DGs and load-shedding location from the best and worst solution.

The best solution presented the value of the objective function of MUS 4.764, with an injection of 2.24 MW in the network and cuts made in the buses, as shown in Tables 5 and 6. In the worst solution, from the six candidate buses found in the constructive phase, only one has load shedding within distribution transformer T11. On the other hand, the best solution includes all six customers for load shedding, where three of them have 20% shedding. Similarly, the worst solution for DGs has only one installed, while the best result includes four DGs.

Table 5. Best solution: DG configuration.

DG_n (bus)	13388	13446	13418	13392	13428	14120
α_n	2	4	4	1	0	3
P_n^G (kW)	320	640	640	160	0	480

Table 6. Best solution: load-shedding setup.

LS_n (bus)	201127	201128	200913	200914	201146	201131
γ_n	5	5	3	3	2	5
X_n	20%	20%	12%	12%	8%	20%

The biggest difference between the worst and best solutions is the number of DG allocations and load shedding, highlighting the importance of implementing such strategies. Nevertheless, the worst and best solutions present very similar locations for load shedding and identical locations for DG installation. Even the worst solution presents attractive positions to install DGs or perform load shedding. Therefore, the difference is related to the number of α_n and γ_n.

As shown in Figure 10, all DG allocations provided by the solution technique are in the medium-voltage network. Likewise, we assume that load shedding must occur in low-voltage buses, which could have high-priority loads. Allowing load shedding in medium-voltage loads could lead the metaheuristic to promote only load shedding in such areas.

Most found solutions have allocated a DG close to the substation, except for a DG at bus 14120. A DG installed far from the substation promotes a relevant increase in the voltage profile, according to the DG's capacity. On the other hand, the allocation of DGs close to the substation provides a low increase in the voltage profile. The solution

technique seeks to install more DGs close to the substation to minimize energy losses and, simultaneously, to avoid overvoltage problems.

As indicated in Table 5, none of the generators has $\alpha_n = \overline{\alpha}$ due to the impact on the system's voltage profile. The solution technique identified a more suitable setup when using smaller-capacity generators to avoid overvoltage problems.

The loads downstream of transformers T17 and T26 are shown in Figure 11, highlighting the main areas with load shedding. Three load sheddings were considered in the same buses for both worst and best solutions. The worst case has $\gamma_n = 0$ for loads 200914, 201128, and 201131, while the best case has $\gamma_n = 3$, 5, and 5, respectively. The constructive process finds initial solutions, and the local search refines their quality, maintaining good quality of load-shedding locations, even for the worst solution.

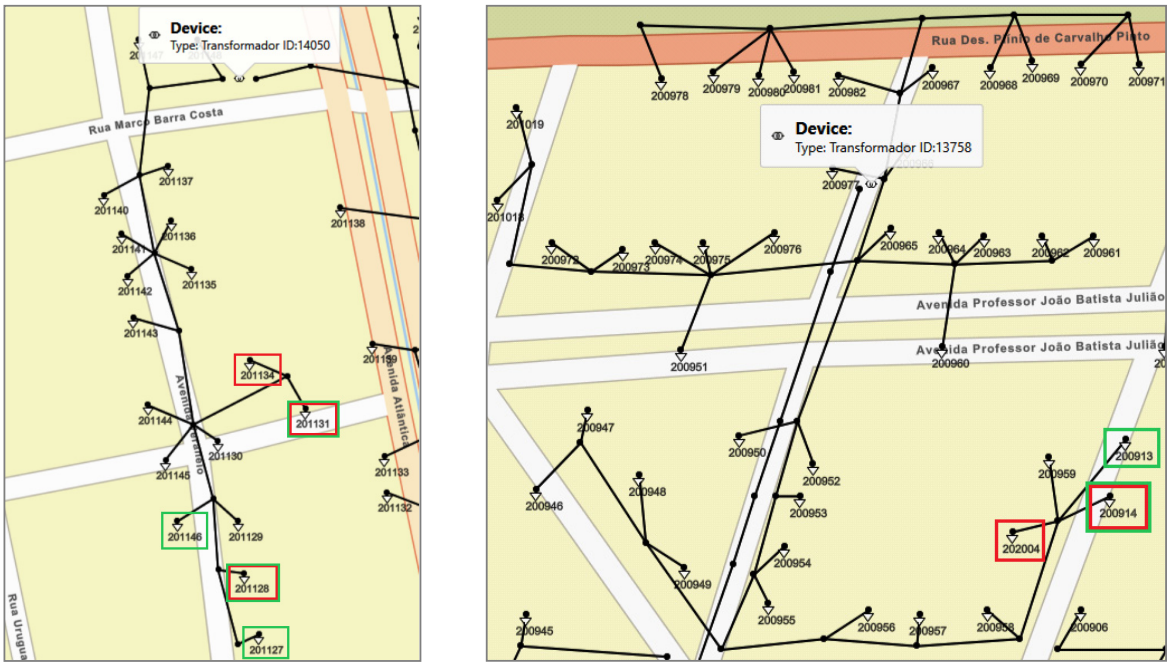

(**a**) (**b**)

Figure 11. Details from loads in (**a**) TR17 and (**b**) TR26.

Figure 12 shows the voltage profile of the initial condition or base case (orange marks) and the best solution (blue marks). The voltage difference between phases is small. However, solving the problem of managing the capacity considering unbalanced smart grids may provide a more appropriate solution than works without such an important aspect.

As shown in Figure 12, allocating DGs in the distribution network increases the voltage levels up to 2.02% at the bus 200800 within distribution transformer T11 due to the combined optimization of DG allocation simultaneously with load shedding, reliability indices, load transference, and the possibility of islanded operation. Such voltage improvement provides power loss reduction. Phase C in the base case presents the lower voltage levels. Nevertheless, DG allocation and load shedding in the best solution provide the best voltage improvement for the same phase.

The proposed solution allocates the generators in regions where the generators can supply the loads and perform islanded operations during fault events. So, including reliability optimization aspects in the objective function increases the overall benefits from optimal allocation and sizing of DGs and load shedding.

The results show that all parts of the objective function work cooperatively to increase response demand and reliability. For instance, the islanded operation is improved when load allocation and load shedding are considered simultaneously. The implementation of generators allows islanding, while load shedding increases the chances of success of the

islanded operation, reducing the demand in the region that will be islanded and increasing reliability and customer satisfaction.

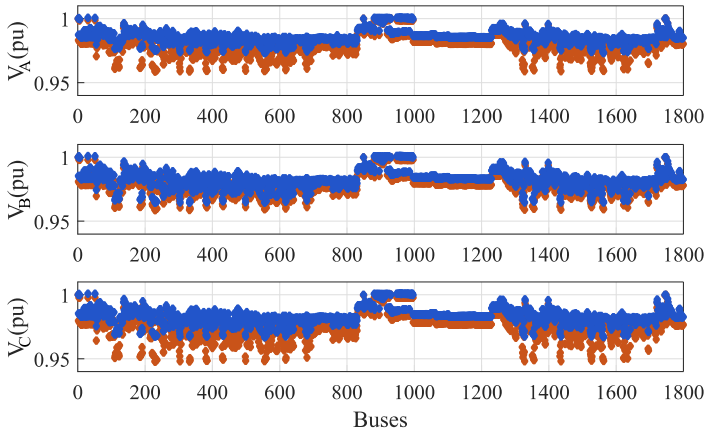

Figure 12. Voltage profile for different cases.

5. Conclusions

This work applied a methodology based on the hybrid GRASP and TS algorithm to evaluate the effects of the optimal allocation of DGs and load shedding in the smart grid while also considering reliability aspects. The results show that the objective function produces a higher value if load shedding is not carried out together with the optimal DG allocation. Optimal benefits from DG and load shedding can be achieved by conducting adequate planning to determine the most suitable bus for minimum shedding, as well as the ideal size and location of DGs, which may vary depending on the system.

The results found highlight the advantages of performing demand-side management, ensuring a better distribution of the load curve. The benefits include a better voltage profile and network capacity relief. Load restoration is also increased by the islanded operation and load transference to neighbor feeders. Load shedding benefits load restoration as well. The combination of these techniques allows for enhancing reliability indices and, consequently, energy quality to customers.

Most DGs installed by the proposed method are closer to the substation. Such an aspect highlights the challenges of the massive integration of DGs into the distribution network. Massive DG placement increases voltage levels and may surpass the voltage upper limit imposed by regulatory agencies. Thus, the proposed method allocates the DGs near the substation to ensure compliance with these limits. Furthermore, although there is a slight voltage difference between phases, the previous conclusions highlight that solving the problem of managing the capacity considering unbalanced smart grids may provide a more appropriate solution than works without such an important aspect.

Distribution networks with degraded voltage profiles can benefit more from the proposed methodology. In this scenario, the DG installation will be larger and better distributed along the distribution network. Thus, the number of restored loads can increase, benefiting reliability indices as well.

Further studies should consider the existence of critical loads into feeder sections, enforcing different rewards to demand response programs and, consequently, improving DSM. Tools for improving distribution network performance should be integrated into the model, such as smart inverters of electronically coupled DGs that can already be installed in the distribution network and belong to a private owner. Furthermore, integrating some technologies, such as energy storage systems, may require future modifications in the proposed method since such a device requires evaluating the energy balance to support the islanded operation of microgrids.

Author Contributions: Conceptualization, H.d.O.M.S. and J.B.L.; Investigation, H.d.O.M.S. and C.R.; Methodology, H.d.O.M.S., C.R. and J.B.L.; Software, H.d.O.M.S., C.R. and J.B.L.; Supervision, J.B.L.; Validation, H.d.O.M.S. and C.R.; Writing—original draft, H.d.O.M.S. and C.R.; Writing—review and editing, C.R. and J.B.L. All authors have read and agreed to the published version of the manuscript.

Funding: This paper was possible thanks to the scholarship granted from the Brazilian Federal Agency for Support and Evaluation of Graduate Education (CAPES)—Finance code 001, and the São Paulo Research Foundation (FAPESP), grants 2015/21972-6 and 2019/07436-5.

Institutional Review Board Statement: This study did not require ethical approval.

Data Availability Statement: There is no additional data beyond that provided throughout the article.

Conflicts of Interest: The authors declare no conflict of interest.

Nomenclature

C^{ENS}	Cost of energy not supplied in monetary unit.
C^{LOSS}	Cost of power losses in monetary unit.
C^{SHED}	Cost of load shedding in monetary unit.
C_k^{ENERGY}	Energy price according to the type of customer, USD/kWh.
C_k^{SHED}	Cost of load shedding to k-th type of customer, USD/kW, which can be residential, R, commercial, C, or industrial, I.
$I_{j,p,y}$	Current flow through the j-th distribution line at p-th phase, A.
$I_{p,i,y}$	Current injected in the i-th bus, phase p, A.
L_h	Line length of the branch h, km.
$P_{i,p,k,y}^{MAX}$	Maximum cuttable power in i-th bus and p-th phase, kW.
$P_{i,y,m}^{MG}$	Loads belonging to the microgrid m in section i, year y that cna be restored, kW.
$P_{i,y}^{MG}$	Microgrids' loads in section i, year y that can be restored, kW.
$P_{i,y}^{TS}$	The sum of transferred loads downstream automatic tie switches in section i, year y, kW.
$P_{i,y}^{p}$	Total loads in the section i and down-stream, year y, kW.
$P_{p,i,y}$	Active power injected in the i-th bus, phase p, kW.
$P_{p,i,y}^{D}$	Active power demand in the i-th bus, phase p, kW.
$P_{p,i,y}^{DG}$	Active power injected by the DG in the i-th bus, phase p, kW.
P_y^{ENS}	Energy not supplied during permanent faults for each year y, kW.
$Q_{p,i,y}$	Reactive power injected in the i-th bus, phase p, kVAr.
$Q_{p,i,y}^{D}$	Reactive power demand in the i-th bus, phase p, kVAr.
$Q_{p,i,y}^{DG}$	Reactive power injected by the DG in the i-th bus, phase p, kVAr.
$R_{j,p}$	Line resistance of the j-th distribution line, phased p, Ω.
T_{SW}	The time of power outage necessary to the system operator restores the loads by using automatic switches, s.
$V_{p,i,y}$	Voltage magnitude of the i-th bus, phase p, pu.
$X_{i,p,k,y}$	Percentage of load shedding in the bus i, phase p, costumer type k.
$X_{j,y}$	Percentage of load shedding in the candidate bus n.
k_e	Cost of losses, USD/kWh.
t_R^p	The duration of power outages caused by permanent faults, s.
$\alpha_{j,y}$	Integer multiplying factor of the base value for the DG power capacity.
$\beta_{j,y}$	Integer multiplying factor of the power factor base value.
$\gamma_{j,y}$	Integer multiplying factor of the load shedding base value.
λ_h^p	Failure rate of line h per kilometer year.
$\boldsymbol{\pi}_i$	Set of branches belonging to section i.
$\boldsymbol{\sigma}_m$	Set of branches belonging to the microgrid m.
$\boldsymbol{\tau}_w$	Set of branches belonging to the microgrid m.
ΔX	Base value of the load shedding.
Δpf	Base value of the power factor.
IRR	Internal rate of return.
$g(c)$	Greedy function to assess the candidate solution c.
ΔP^{DG}	Base value of the DG power capacity, kW.
$\boldsymbol{\beta}$	Set of all sections defined by the protection and control devices.
$\boldsymbol{\varphi}$	Set of year of the planning horizon.

References

1. Carr, J.A.; Balda, J.C.; Mantooth, H.A. A Survey of Systems to Integrate Distributed Energy Resources and Energy Storage on the Utility Grid. In Proceedings of the 2008 IEEE Energy 2030 Conference, Atlanta, GA, USA, 17–18 November 2008; pp. 1–7.
2. Blokhuis, E.; Brouwers, B.; van der Putten, E.; Schaefer, W. Peak Loads and Network Investments in Sustainable Energy Transitions. *Energy Policy* **2011**, *39*, 6220–6233. [CrossRef]
3. Wang, J.; Lu, X.; Chen, C. *Guidelines for Implementing Advanced Distribution Management Systems-Requirements for DMS Integration with DERMS and Microgrids*; Argonne National Lab (ANL): Argonne, IL, USA, 2015.
4. Jabir, H.; Teh, J.; Ishak, D.; Abunima, H. Impacts of Demand-Side Management on Electrical Power Systems: A Review. *Energies* **2018**, *11*, 1050. [CrossRef]
5. Limaye, D.R. Implementation of Demand-Side Management Programs. *Proc. IEEE* **1985**, *73*, 1503–1512. [CrossRef]
6. Gellings, C.W. The Concept of Demand-Side Management for Electric Utilities. *Proc. IEEE* **1985**, *73*, 1468–1470. [CrossRef]
7. Hayes, B.; Hernando-Gil, I.; Collin, A.; Harrison, G.; Djokic, S. Optimal Power Flow for Maximizing Network Benefits From Demand-Side Management. *IEEE Trans. Power Syst.* **2014**, *29*, 1739–1747. [CrossRef]
8. Dehnavi, E.; Abdi, H. Determining Optimal Buses for Implementing Demand Response as an Effective Congestion Management Method. *IEEE Trans. Power Syst.* **2016**, *32*, 1537–1544. [CrossRef]
9. Saffre, F.; Gedge, R. Demand-Side Management for the Smart Grid. In Proceedings of the 2010 IEEE/IFIP Network Operations and Management Symposium Workshops, Osaka, Japan, 19–23 April 2010; pp. 300–303.
10. U.S. Department of Energy. *Benefits of Demand Response in Electricity Markets and Recommendations for Achieving Them*; U.S. Department of Energy: Washington, DC, USA, 2006.
11. Zhang, S.; Cheng, H.; Wang, D.; Zhang, L.; Li, F.; Yao, L. Distributed Generation Planning in Active Distribution Network Considering Demand Side Management and Network Reconfiguration. *Appl. Energy* **2018**, *228*, 1921–1936. [CrossRef]
12. Zhang, H.; Gong, C.; Ju, W.; Pan, G.; Wang, W. Optimization Dispatch Modeling for Demand Response Considering Supply and Demand Balance and Security Constraints. In Proceedings of the 2021 Power System and Green Energy Conference (PSGEC), Shanghai, China, 20–22 August 2021; pp. 166–170.
13. Arun, C.; Aswinraj, R.; Bijoy, M.T.; Nidheesh, M.; Rohikaa Micky, R. Day Ahead Demand Response Using Load Shifting Technique in Presence of Increased Renewable Penetration. In Proceedings of the 2022 IEEE 7th International conference for Convergence in Technology (I2CT), Mumbai, India, 7–9 April 2022; pp. 1–6.
14. Abideen, M.Z.U.; Ellabban, O.; Ahmad, F.; Al-Fagih, L. An Enhanced Approach for Solar PV Hosting Capacity Analysis in Distribution Networks. *IEEE Access* **2022**, *10*, 120563–120577. [CrossRef]
15. Sarwar, S.; Mokhlis, H.; Othman, M.; Shareef, H.; Wang, L.; Mansor, N.N.; Mohd Khairuddin, A.S.; Mohamad, H. Application of Polynomial Regression and MILP for Under-Frequency Load Shedding Scheme in Islanded Distribution System. *Alex. Eng. J.* **2022**, *61*, 659–674. [CrossRef]
16. Sapari, N.M.; Mokhlis, H.; Laghari, J.A.; Bakar, A.H.A.; Dahalan, M.R.M. Application of Load Shedding Schemes for Distribution Network Connected with Distributed Generation: A Review. *Renew. Sustain. Energy Rev.* **2018**, *82*, 858–867. [CrossRef]
17. Awad, H.; Hafez, A. Optimal Operation of Under-Frequency Load Shedding Relays by Hybrid Optimization of Particle Swarm and Bacterial Foraging Algorithms. *Alex. Eng. J.* **2022**, *61*, 763–774. [CrossRef]
18. Mitra, J.; Vallem, M.R.; Singh, C. Optimal Deployment of Distributed Generation Using a Reliability Criterion. *IEEE Trans Ind. Appl.* **2016**, *52*, 1989–1997. [CrossRef]
19. Atwa, Y.M.; El-Saadany, E.F.; Salama, M.M.A.; Seethapathy, R. Optimal Renewable Resources Mix for Distribution System Energy Loss Minimization. *IEEE Trans. Power Syst.* **2010**, *25*, 360–370. [CrossRef]
20. Dang, C.; Wang, X.; Wang, X.; Li, F.; Zhou, B. DG Planning Incorporating Demand Flexibility to Promote Renewable Integration. *IET Gener. Transm. Distrib.* **2018**, *12*, 4419–4425. [CrossRef]
21. Shekari, T.; Gholami, A.; Aminifar, F.; Sanaye-Pasand, M. An Adaptive Wide-Area Load Shedding Scheme Incorporating Power System Real-Time Limitations. *IEEE Syst. J.* **2018**, *12*, 759–767. [CrossRef]
22. Reiz, C.; De Lima, T.D.; Leite, J.B.; Javadi, M.S.; Gouveia, C.S. A Multiobjective Approach for the Optimal Placement of Protection and Control Devices in Distribution Networks with Microgrids. *IEEE Access* **2022**, *10*, 41776–41788. [CrossRef]
23. Resende, M.G.C.; Ribeiro, C.C. Greedy randomized adaptative search procedures: Advances and extensions. In *Handbook of Metaheuristics*; Springer: New York City, NY, USA, 2019; Chapter 6; pp. 169–220.
24. Glover, F.L.M. *Handbook of Combinatorial Optimization*; Springer: Boston, MA, USA, 1998; Volume 3.
25. Laboratory of Electrical Power System Planning—LAPSEE. Distribution Testing System of 1806 Buses. Available online: https://www.feis.unesp.br/Home/departamentos/engenhariaeletrica/lapsee807/home/distribution_network_1806_lines.rar (accessed on 30 November 2022).